ADVANCED FUNCTIONAL MATERIALS
www.afm-journal.de

# Structured Multilayer Thin Films for Catalytic Applications: A Novel Approach on Catalyst Design Utilizing Microfabrication Techniques

*Shivam Shivam,* Mudassar Javed, Georg Brösigke, Jens-Uwe Repke, Lukas Thum, Roel van de Krol, Iver Lauermann, Rutger Schlatmann, Albert Gili, and Daniel Amkreutz*

**The metal/metal oxide interface is key to establishing catalytic performance, selectivity, and stability in heterogeneous systems. In this proof-of-concept study, a systematic methodology is introduced for the preparation of multilayer catalysts that combines Radio Frequency (RF) magnetron sputtering with laser microstructuring for the synthesis of high-density Cu/ZnO interfaces. By means of a specifically designed split target, alternating few-nanometer-thick layers of Cu and ZnO are deposited under precise control and with high reproducibility. Laser scribing is then employed to create defined microstructures that reveal buried interfaces, improving access to catalytically active interfaces. As-deposited and laser-scribed multilayer's structural and chemical stability is confirmed through Atomic Force Microscopy (AFM), X-Ray Fluorescence (XRF), X-Ray Diffraction (XRD), X-Ray Photoelectron Spectroscopy (XPS), and Scanning Electron Microscope (SEM) characterizations. Catalytic activity is evaluated under gradient-free, continuous-stirring conditions for $CO_2$ hydrogenation to methanol where the catalyst produces methanol and CO under laboratory-scale conditions. The strategy addresses specific design bottlenecks such as limited control over interfacial geometry and exposure while acknowledging the inherent limitations of thin-film systems in terms of surface area and scalability. While demonstrated for $CO_2$-to-methanol conversion, the method is generally applicable to other interface-dependent reactions. Building on this initial demonstration, forthcoming efforts will focus on detailed mechanistic analysis, long-duration testing, and performance benchmarking against conventional powder-based catalysts.**

## 1. Introduction

The design and optimization of heterogeneous catalysts play a pivotal role in addressing global challenges such as $CO_2$ mitigation, and sustainable chemical production.[1] Among these, $CO_2$ hydrogenation to methanol has garnered significant attention due to its dual benefit of reducing greenhouse gas emissions and producing methanol—a key chemical building block used for energy storage, as a transport medium, and as a potential fuel alternative.[2,3] However, this reaction presents several challenges, including balancing catalytic activity, selectivity, and stability under industrially relevant conditions.[4]

Conventional methods for catalyst preparation, such as co-precipitation or impregnation, often suffer from poor control over the interface and composition, which are critical for catalytic activity and selectivity.[5] Recent advances in metal/metal oxide interface engineering have highlighted the importance of interfacial design in tuning catalytic activity and stability.[6,7] A recent study on Pd thin-film catalysts for acetylene hydrogenation illustrated how planar 2D catalyst architectures with engineered

S. Shivam, L. Thum, I. Lauermann, R. Schlatmann, A. Gili, D. Amkreutz
PVcomB
Helmholtz Zentrum Berlin für Materialien und Energie
Schwarzschildstraße 3, 12489 Berlin, Germany
E-mail: shivam.shivam@helmholtz-berlin.de

The ORCID identification number(s) for the author(s) of this article can be found under https://doi.org/10.1002/adfm.202514003



**DOI: 10.1002/adfm.202514003**

M. Javed, G. Brösigke, J.-U. Repke
Process Dynamics and Operations Group
Technische Universität Berlin
Straße des 17. Juni 135, 10623 Berlin, Germany

S. Shivam, R. van de Krol
Institut für Chemie
Technische Universität Berlin
Straße des 17. Juni 124, 10623 Berlin, Germany

R. van de Krol
Institute for Solar Fuels
Helmholtz Zentrum Berlin für Materialien und Energie
Hahn-Meitner-Platz 1, 14109 Berlin, Germany

functional and reactive interfaces can deliver high productivity and selectivity. These systems leverage subsurface and lateral interactions, typically inaccessible in conventional catalysts to form self-regenerating catalytic phases and mitigate deactivation, offering a new route for scalable and efficient catalyst design.[8] Similarly, Zhang et al. demonstrated temperature-dependent active site regulation in photothermocatalytic $CO_2$ hydrogenation, emphasizing the importance of interfacial design to achieve optimal performance.[9] These studies underline the potential of catalytically active interface, such as Cu-ZnO, to enhance methanol selectivity and catalytic stability by leveraging synergistic effects at the metal/metal-oxide interface.[10]

For some reactions, the interaction between a metal and metal oxide results in catalytic performance that far exceeds the capabilities of either component alone.[11] At these interfaces, electronic interactions modify the metal's electronic structure, enabling efficient charge transfer and activation of reactants.[12] Another contributing factor is the spillover concept, in which the oxide component stabilizes intermediates and favours specific reaction pathways, while the metal dissociates and activates key species like hydrogen or oxygen.[13] Moreover, as highlighted by Zou et.al[14] these interfaces are not static but undergo dynamic transformations under reaction conditions. These changes enable the catalyst to adapt to the chemical environment, potentially enhancing reactant activation and intermediate stabilization. However, such transformations do not always lead to optimal performance, as they may also contribute to catalyst deactivation over time. This dynamic behavior highlights how interface adaptability can simultaneously enhance activity and contribute to deactivation, highlighting the importance of precise interface engineering to balance these effects. Frei et al. demonstrated that pure copper shows minimal activity in the hydrogenation of $CO_2$ to methanol. This catalytic transformation is predominantly facilitated by the interface between Cu and ZnO, resulting in an activity increase by a factor of 100 on a single interface thin film system compared to either material in isolation, yet achieving scalable and reproducible fabrication of such interfaces remains a challenge.[15]

Another critical issue is the structural and chemical stability of catalysts under harsh reaction conditions. As deactivation can occur through mechanisms such as poisoning and sintering. Poisoning, where impurities bind strongly to active sites, inhibits catalytic activity; a notable example is sulfur poisoning in nickel catalysts during hydrocarbon hydrogenation.[16] Sintering, the agglomeration of metal nanoparticles at high temperatures, reduces active surface area and catalytic performance, as observed in iron catalysts used for ammonia synthesis[17] or nickel catalysts for the dry reforming of methane.[18] These challenges have prompted the exploration of more thermally and chemically robust catalytic systems, including oxide-based materials such as $In_2O_3$, which retain their crystallographic integrity under demanding reaction conditions.[19] In parallel, recent advances in catalyst design have focused on stabilizing the active sites by engineering robust interfaces between metal and metal-oxide supports, such as Cu-ZnO, which is widely regarded as the active site for methanol synthesis.[20] These sites play a pivotal role in adsorbing reactant molecules, stabilizing transient reaction intermediates, and guiding complex chemical transformations toward the desired products.[21]

In this work, we introduce a proof-of-concept methodology to construct and expose Cu–ZnO interfaces using a combination of thin-film deposition and laser structuring. Although thin-film systems are not inherently designed for large-scale catalytic deployment due to their limited surface area, they offer unparalleled precision in constructing and accessing interfacial regions. This study focuses on the synthesis and structural validation of multilayer architectures and their interface exposure via laser scribing. Rather than replacing conventional high-surface-area powder catalysts, our approach is intended to provide a controllable and reproducible platform to probe interface effects, optimize design principles, and serve as a model system for future catalytic studies. The concept is demonstrated for a chemical reaction of high importance for the energy transition: $CO_2$ hydrogenation to methanol on precisely engineered Cu-ZnO interface. Using a conventional RF magnetron sputtering system with a custom build split target, we are able to deposit hundreds of alternating layers of Cu and ZnO on corning glass by placing the sample off-center and rotating the substrate carrier after a defined time period by 180°. Afterwards, a picosecond laser was employed to create microstructures, exposing the interfaces for gas phase reaction to take place. This approach offers a novel and effective strategy to enhance the accessibility of catalytically active sites in heterogeneous catalysts by leveraging the key advantages of picosecond laser scribing over traditional photolithography. Unlike photolithographic techniques that require cleanroom environments, photomasks, chemical etchants, and multiple fabrication steps, laser scribing is a maskless, contactless, and direct-write process. This significantly simplifies the fabrication workflow while offering high spatial precision and patterning flexibility. Importantly, laser scribing is fully compatible with scalable thin-film deposition methods such as RF magnetron sputtering and can be readily integrated with roll-to-roll manufacturing platforms. Furthermore, while previous studies focused on single-interface systems, our method enables the construction of multilayered architectures with up to 250 alternating Cu/ZnO layers. This stacking strategy results in a substantial increase in interfacial density, achieving values comparable to those reported using complex photolithographic processes. These features position our method as a scalable, rapid, and versatile alternative for fabricating interface-rich model catalysts. While this study focuses on demonstrating the feasibility of the approach, future work will aim to assess long-term stability, investigate mechanistic aspects, and benchmark performance against conventional powder-based catalyst systems.

## 2. Results and Discussion

The first step in our method design was to study the effect of sample positioning in the sputtering chamber on the composition and thickness of the resulting single layers. This step was critical because a split target with distinct Cu and ZnO segments was used, which introduces inherent spatial variations in deposition dynamics. Understanding how these variations influence the film composition and thickness is essential for optimizing the deposition process and achieving well-defined layers. (**Figure 1a**) shows a schema of the positioning of the samples in the deposition chamber, below the target. XRF proves that the composition of films is dependent on the position of the samples on the

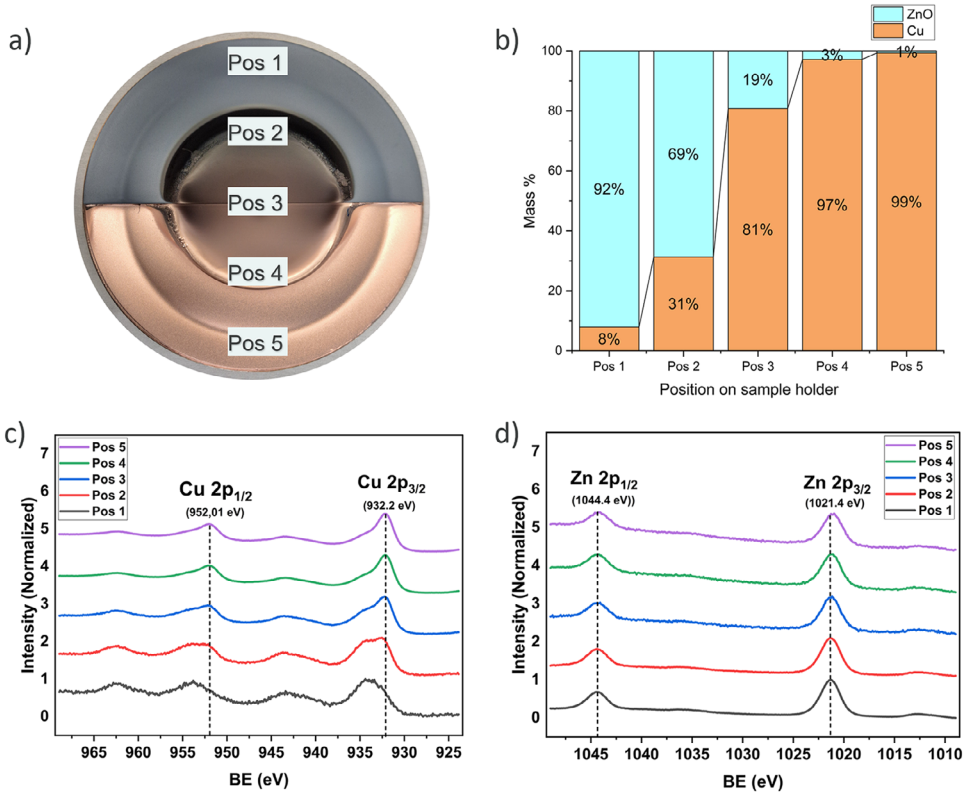


**Figure 1.** a) Image of the target with added position of samples on sample holder for static deposition/single layer; b) Mass % of Cu and ZnO in static deposited samples as a function of the position obtained from XRF; c) Cu 2p spectra of samples at various positions showing variation in oxidation state of Cu obtained from XPS; d) ZnO 2p spectra of samples at various positions showing variation in oxidation state of ZnO obtained from XPS.

sample holder (Figure 1b). At Pos 1, the film is predominantly ZnO (wt.% = 92%) due to its direct alignment with the ZnO segment of the split target, resulting in minimal Cu deposition. Conversely, at Pos 5, the film is nearly pure Cu (wt.% = 99%) because of its proximity to the Cu segment, with negligible ZnO contribution. At Pos 3, a central position between the two segments, the composition is Cu-rich (Cu wt.% = 81%, ZnO wt.% = 19%): this can be attributed to Cu's higher sputtering yield and broader angular distribution lead to a faster deposition rate compared to ZnO.[22] The residual Cu content of ≈8% in the ZnO layer at Pos 1 deserves attention, particularly in the context of its potential impact on catalytic performance. This corresponds to a local Cu/Zn molar ratio of ≈0.08 within the ZnO phase, as detected by our measurements. While this is significantly lower than the overall Cu/Zn ratios of 1:1 to 3:1 typically found in bulk compositions of industrial Cu/ZnO-based methanol synthesis catalysts, it highlights the minor but measurable intermixing of Cu into the ZnO layer in our system. Industrial catalysts require higher Cu wt% (33% to 75%) to provide sufficient active sites for $CO_2$ hydrogenation, while ZnO primarily acts as a structural support to enhance Cu dispersion and facilitate electronic interactions. In the case of our multilayer system, the catalytic activity will largely arise from the well-defined Cu-ZnO interfaces, where the synergy between the two materials is most effective and can provide the necessary Cu/Zn molar ratio for effective interfacial catalytic activity. The minor Cu content within the ZnO layer is unlikely to contribute significantly to catalytic activity but does not compromise the structural or functional integrity of the multilayer system. Cu 2p and ZnO 2p spectra obtained from XPS revealed the variation in oxidation states of these statically deposited samples (Figure 1c,d). The Cu 2p spectra indicates that depositing with a split target containing ZnO as an oxygen source leads to a gradual change in the oxidation state of Cu along the deposition axis, transitioning from the ZnO to the Cu segment of the target. Peak positions for the Zn 2p spectra of the samples deposited directly beneath the Cu segment of the target show a small shift but the relative difference between Zn $2p_{3/2}$ and Zn $2p_{1/2}$ is the same, which is in line with the published literature.[23] Based on these findings and to ensure minimal cross intermixing between layers, samples placed in Pos 1 and Pos 5 were further used in this work.

Surface roughness and its propagation in multilayered thin films poses a critical challenge that must be addressed. This is particularly important in other fields such as solar cells and optical coatings.[24,25] For catalytic systems, such as Cu-ZnO multilayers, roughness may affect the interaction between layers, active site distribution, and overall catalytic performance-:a well-defined and smooth interface is desirable and control over roughness propagation is needed.

First, the surface roughness as a function of the layer thickness of individual layers was studied using AFM and is shown in **Figure 2**. Our observations indicate that in the case of the Cu film, an increase in thickness from 20 to 50 nm leads to an increase in the RMS roughness from 0.3 to 1.4 nm. This phenomenon

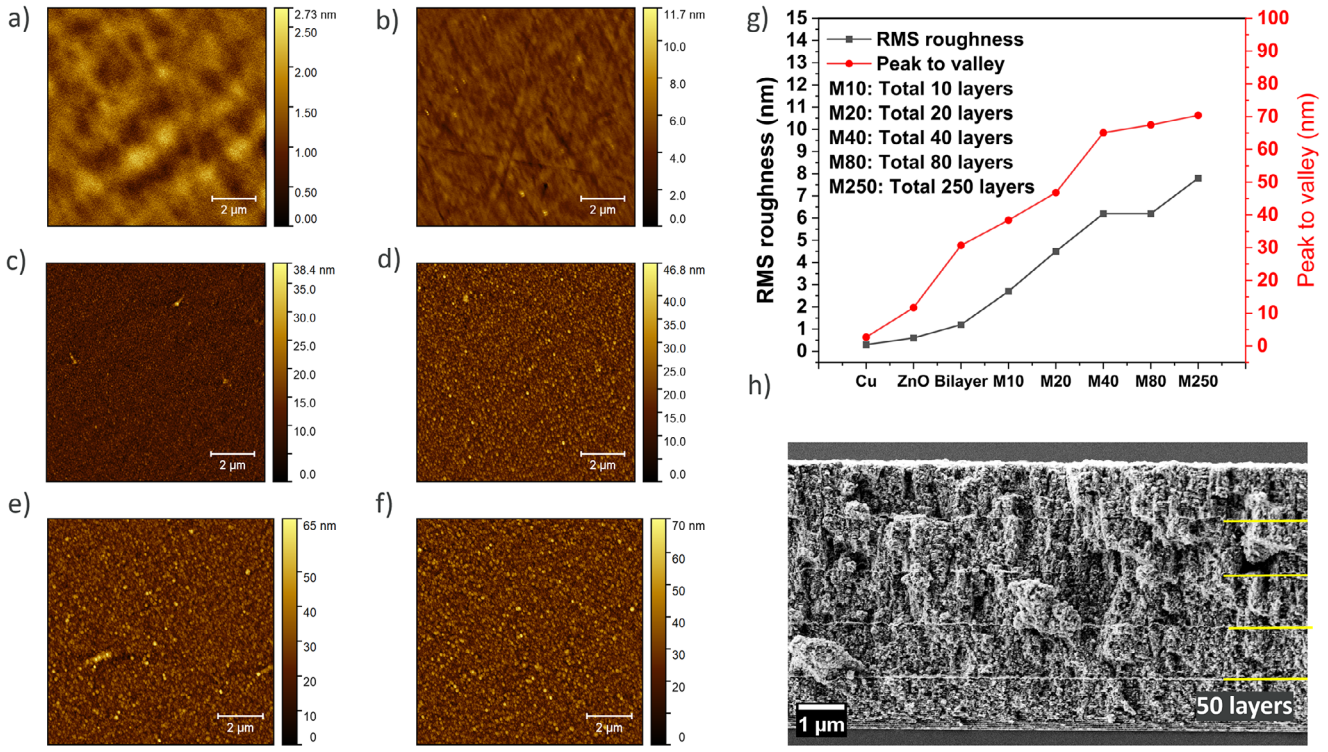


**Figure 2.** Surface morphology and roughness evolution of Cu/ZnO thin films with increasing layer repetitions. a–f) 3D AFM images (10 × 10 µm$^2$ scan area) showing surface morphology of (a) 20 nm Cu, (b) 20 nm ZnO, (c) M10 (d) M20 (e) M40 (f) 250, (g) Evolution of RMS roughness and peak-to-valley height with increasing number of Cu/ZnO layers (M10–M250). h) As deposited multilayer with Cu interlayer(marked in yellow for reference).

can be attributed to the uniform propagation of similarly sized crystallites throughout the film. When the thickness is increased, more crystallites are formed, contributing to a more uneven surface topography.[26] Similarly, for the ZnO layer, an increase in thickness from 20 to 50 nm results in an increase of RMS roughness from 0.6 to 1.5 nm. This effect is primarily driven by the expansion of grain size within the layer. Fewer grain boundaries and a more uniform surface emerge because of these enlarged grains.[27,28] But on comparing both samples for same thickness, the ZnO film was rougher in comparison to Cu films, likely due to the different crystallite growth mechanisms between the $Fm\bar{3}m$ structure of Cu and the $P6_3mc$ structure of ZnO.[26–29] Scaling up the study of surface roughness to multilayer samples, AFM revealed that with increase in number of layers the roughness also increases (Figure 2a–f, more details in Table S1, Supporting Information).

A comprehensive analysis of the surface morphology and roughness evolution in Cu/ZnO multilayer thin films as the number of bilayers increases. AFM images (a–f) reveal a progressive increase in surface roughness. This trend is quantitatively captured in panel (g), where both RMS roughness and peak-to-valley height increases with bilayer repetitions, indicating roughness accumulation over successive depositions. While a thick (100 nm) Cu interlayer was introduced after every 50 layers in the M250 sample (visualized in the cross-sectional SEM image, Figure 2h), it primarily serves as a visual marker to segment the multilayer structure. Despite the pronounced waviness, the RMS roughness remains below the individual layer thickness (20 nm), ensuring that the Cu and ZnO layers remain distinguishable and do not intermix. This validates the feasibility of constructing 250-layer architectures with preserved layer integrity, albeit with increased surface topography.

Once multilayers are deposited, the interface of Cu and ZnO needs to be exposed for gas phase reaction. This was achieved by creating microstructures using a picosecond laser with a Gaussian beam profile,[30,31] as schematically shown in **Figure 3**a. For this, 2 approaches were pursued a) continuous scribing for cuboidal structures b) pulsed scribing for circular holes also termed as inverse structures as seen in Figure 3b,c. The ultrashort pulse duration ensures an adiabatic laser–material interaction, leading to rapid vaporization of the material at the focal point. This ensures minimal heat diffusion to the surrounding regions, thereby preserving the structural integrity of the adjacent multilayers.

The edge length/ diameter to pitch (edge to edge distance between two structures) ratio was kept equal to 1 for both approaches. Figure 3b illustrates that decreasing the pitch between circular holes in a hexagonal array substantially increases interfacial density. The shaded region in the figure highlights the design space relevant to this study, corresponding to microstructures with dimensions ≈ 100 µm: selected based on the resolution limits of the current laser structuring setup. Although the total geometric surface area is low, the edges of the laser-scribed holes expose buried Cu–ZnO interfaces known to be catalytically active. The focus here is not on maximizing surface area but on controlled interface exposure. Furthermore, interfacial density can be increased by reducing hole spacing, shrinking hole diameter,

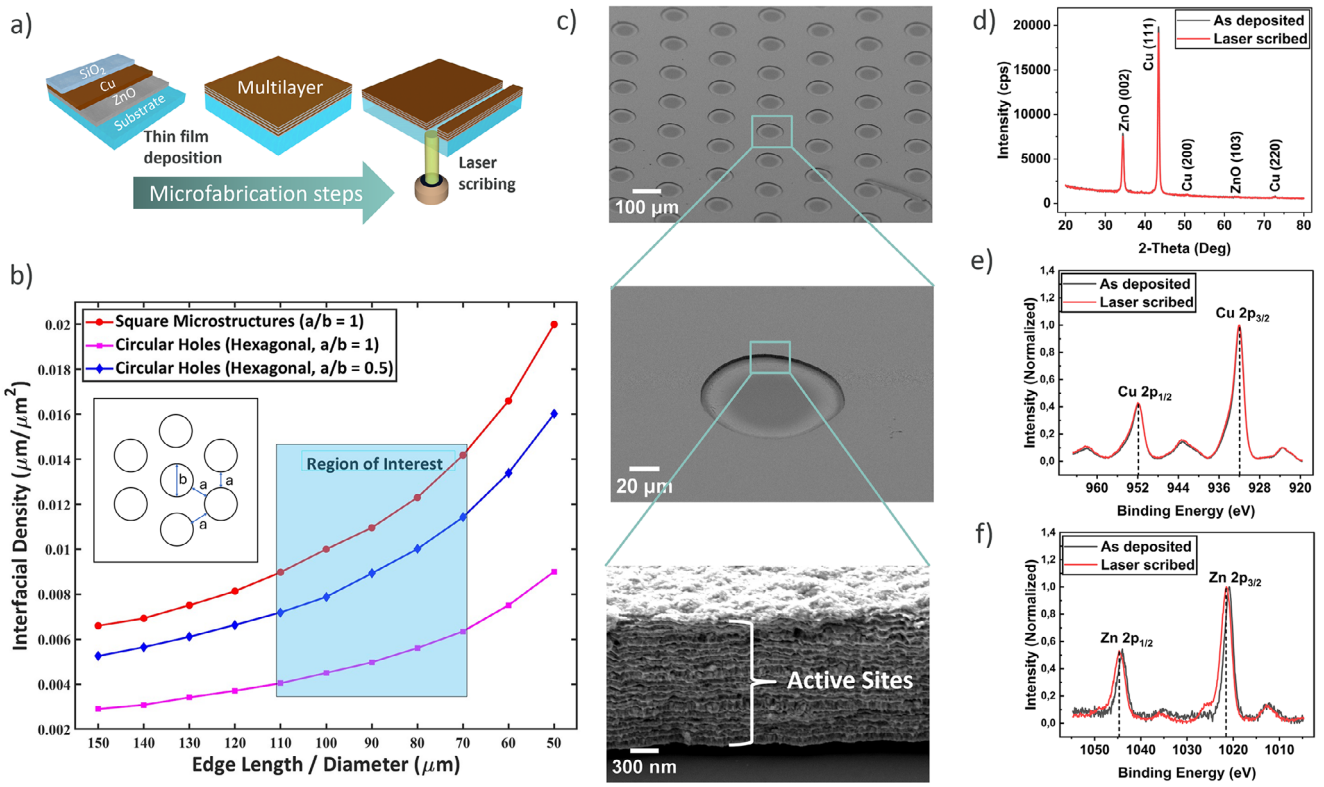


**Figure 3.** a) Schematic representation of the steps of the process. b) Theoretical interfacial density as function of structure dimension for single interface system. c) SEM cross section of laser scribed multilayer. d) XRD diffractogram of the crystal structure before and after laser scribing on multilayer sample. e) XPS spectra, Cu 2p region comparison of before and after laser scribing. f) XPS spectra, Zn 2p region comparison of before and after laser scribing.

or depositing additional bilayers, offering modular tunability for future optimization.

While previous studies, such as those by Frei et al.,[15] focused on single interfaces (i.e., bi-layer systems), our approach involves depositing and structuring 250 layers, significantly enhancing the interfacial density. Given the limitation of structure size in 2D (due to tool constraints), we extended our approach into 3D by adding height to the system through these additional layers. This strategy resulted in a substantial overall increase in interfacial density. To benchmark our results, we compared the interfacial density achieved using our approach with that reported by Frei et al.[15] **Table 1** provides the comparison:

As shown in Table 1, our approach yields an interfacial density of 27400 cm.cm$^{-2}$ (see Note S1, Supporting Information for calculation steps) which is comparable to the highest value previously reported (27700 cm.cm$^{-2}$) for a single-interface system by Frei et al.[15] It is important to note that this comparison relates specifically to interfacial density and accessibility, rather than catalytic productivity, surface area, or cost where conventional powder catalysts maintain key advantages. Although the numerical difference is small, this achievement is particularly noteworthy considering the complexity involved, Frei's structures were realized through photolithography, a highly precise but resource-intensive method requiring cleanroom environments, multiple lithographic and lift-off steps, and stringent control over feature sizes down to 1.5 μm, which is already approaching the resolution limits of UV-based techniques. Moreover, while our current structures are relatively large (e.g., 100 μm), the demonstrated interfacial density suggests substantial room for further improvement. With ongoing optimization of structuring parameters, such as reducing scribed feature sizes, increasing layer count, or altering stacking configurations, our approach holds significant untapped potential for increasing interfacial density, making it a promising platform for fundamental studies and for the development of hybrid or modular catalytic systems that integrate interface control with scalable architectures. X-ray diffraction (XRD) analysis was performed on multilayer samples comprising 20 alternating layers of Cu and ZnO to investigate the impact of laser scribing on the crystal properties and is shown in Figure 3d. Prominent peaks corresponding to ZnO (002), Cu (111), Cu (200), ZnO (103), and Cu (220) were identified at 34.45°, 43.4°, 50.5°, 62.8°, and 73.9°, respectively, in both as-deposited and laser-scribed samples.[32–36] The ZnO peaks were matched to PDF 96-901-1663 ($P6_3mc$), and the Cu peaks to PDF 96-901-2955 ($Fm\bar{3}m$). A comparison between the as-deposited and laser-scribed samples revealed that the intensity profiles of the ZnO

**Table 1.** Comparison of interfacial density with already published literature.

| | Our approach | Single Interface by Frei et al.[15] | |
|---|---|---|---|
| Structure size (diameter, μm) | 100 μm | 50 μm | 1.5 μm |
| Interfacial density (cm.cm$^{-2}$) | 27400 | 800 | 27700 |

and Cu peaks remained largely unchanged. No additional peaks were detected, and no significant peak shifts were observed for any of the reflections. A quantitative comparison of crystallite size and microstrain before and after laser scribing revealed minor structural changes. The ZnO crystallite size decreased slightly from 13.15 nm to 12.92 nm, while Cu decreased from 16.22 nm to 16.18 nm. Correspondingly, microstrain ($\epsilon$) increased marginally from $7.80 \times 10^{-4}$ to $7.94 \times 10^{-4}$ for ZnO, and from $7.90 \times 10^{-4}$ to $7.92 \times 10^{-4}$ for Cu (see Figure S2, Supporting Information for W-H plot). These subtle changes imply minimal surface-level disorder, likely resulting from localized thermal effects during laser processing, while confirming that the overall multilayer crystallinity remains preserved. In addition, XRD measurements were performed on Cu/ZnO multilayers with varying numbers of bilayers namely, M10, M20, M40, and M80 (Figure S3, Supporting Information) to investigate how increasing the layer count influences the structural characteristics. Across all samples, the peak positions remained consistent, signifying minimal stress or strain accumulation within the multilayer stack. However, a clear enhancement in peak intensity, particularly for the Cu (111) and ZnO (002) reflections, was observed with increasing layer number. Furthermore, a visible narrowing of the full width at half maximum (FWHM) for these peaks was noted, indicating improved crystallinity, larger grain sizes, and a lower density of structural defects in samples with more layers. Together, these findings demonstrate that laser scribing preserves the crystalline structure of the multilayers, while increasing the number of bilayers enhances their overall structural order. This improved crystallinity and stability with higher layer counts is particularly advantageous for catalytic applications, as it may support greater thermal and mechanical robustness under prolonged reaction conditions.

To gain further understanding of the effect of the laser scribing process on the surface of the multilayer system, XPS measurements of the Cu 2p and Zn 2p core-levels were also done.

In the Cu 2p region (Figure 3e), the characteristic Cu $2p_{3/2}$ and Cu $2p_{1/2}$ peaks appear at binding energies of 931.9 and 951.8 eV, respectively, and remain consistent across the as-deposited (black curve) and laser-scribed (red curve) samples, indicating that the laser scribing process does not significantly alter the chemical state of Cu.[37,38] In contrast, the Zn 2p region (Figure 3f) shows a noticeable shift in the Zn $2p_{3/2}$ and Zn $2p_{1/2}$ peaks, observed at 1020.8 and 1043.9 eV, respectively, indicating a modified chemical environment for Zn induced by laser scribing.[39–41] This shift in the Zn 2p peaks can be attributed to modifications in the Zn—O bonding environment, potentially caused by the laser scribing process. The localized heating during scribing may lead to bond redistribution or minor structural rearrangements, altering Zn—O bond lengths or coordination states near the surface. Additionally, the laser-induced process could modify interlayer interfaces, causing slight diffusion of elements between the Cu and ZnO layers, which may affect the chemical potential of Zn near the interfaces and contribute to the observed shift.[40] Despite the 0.6 eV shift in the Zn 2p region, the consistent binding energies in the Cu 2p region and the absence of significant peak distortions suggest that the laser scribing process preserves the overall chemical and structural integrity of the multilayer system. These results highlight the suitability of laser scribing as a post-deposition technique for multilayer thin films, with only localized surface effects on the Zn-containing layers.

Interestingly, a similar shift in the Zn 2p peaks (≈0.6 eV) is also observed after thermal treatment of bilayer system at 300 °C (See Note S2; Figure S4b, Supporting Information). This suggests that both laser ablation and thermal annealing induce modifications in the ZnO's chemical environment. In the case of laser ablation, the shift may result from localized heating and bond redistribution at the surface, whereas annealing at 300 °C likely causes a more uniform thermal effect, potentially accompanied by interfacial diffusion or oxygen migration. These similarities point to the sensitivity of ZnO to thermal and laser-induced processes, which primarily affect the Zn—O bonds and the chemical environment of Zn near the surface.

Overall, the consistent positions of the Cu 2p peaks in both experiments indicate that the Cu layer remains chemically stable under laser ablation and annealing conditions. In contrast, the Zn 2p shifts in both cases highlight that ZnO is more susceptible to chemical modifications during these processes. Further investigations using depth profiling would provide greater insight into the extent and nature of these modifications.

Once optimized and characterized along the deposition and laser scribing steps, the multilayer concept was demonstrated for $CO_2$ hydrogenation to methanol in a gradient-free Berty reactor, and the results are shown in **Figure 4a**

Catalytic measurements were conducted for a total Time on Stream (TOS) of ≈20 h, allowing for a preliminary evaluation of short-term structural stability and catalytic activity. While these conditions provide initial insight into performance, extended testing will be required to assess long-term durability and potential deactivation behavior. The results reveal a clear inverse relationship between $CO_2$ conversion and methanol (MeOH) selectivity, as widely reported for this reaction. No measurable catalytic activity was observed at 503 K, and thus this temperature point has been excluded from the reported temperature trend. As the reaction temperature increased from 533 to 563 K, so did the $CO_2$ conversion, reaching a maximum of 0.45% at 563 K. Correspondingly, the rate of methanol formation was measured at $4.7 \times 10^{-12}$ $mol_{MeOH}.min^{-1}.cm^{-1}{}_{interface}$ which represents a substantial enhancement compared to the rate reported by Frei et al.[15] for a single-interface system of 100 $nmol.h^{-1}cm^{-2}{}_{Cu}$. For the sake of direct comparison their rate was converted to $2.08 \times 10^{-16}$ $mol_{MeOH}.min^{-1}.cm^{-1}{}_{interface}$. This improvement stems from the higher interfacial density enabled by our fabrication method, which increased from 0.08 $\mu m.\mu m^{-2}$ in the reference system to 2.74 $\mu m.\mu m^{-2}$**)** in our structured multilayer system. Despite the modest $CO_2$ conversion observed, the resulting Space-Time Yield (STY) of the structured multilayer catalyst was approximately 0.078 $g_{MeOH}.g\_cat^{-1}.h^{-1}$, based on the methanol formation rate and a total catalyst loading of 39 mg. This value reflects the proof-of-concept nature of the current system, which was designed to emphasize interfacial architecture and controlled exposure over total active surface area. In comparison, conventional $Cu/ZnO/Al_2O_3$ powder catalysts typically exhibit STY values in the range of 0.2 to 1 $g_{MeOH}.g\_cat^{-1}.h^{-1}$ under optimized high-pressure conditions.[42,43] The lower STY in our multilayer system can be attributed to several factors, including limited interface accessibility per unit reactor volume, absence of traditional promoters (e.g., $Al_2O_3$ or $Ga_2O_3$), and

 

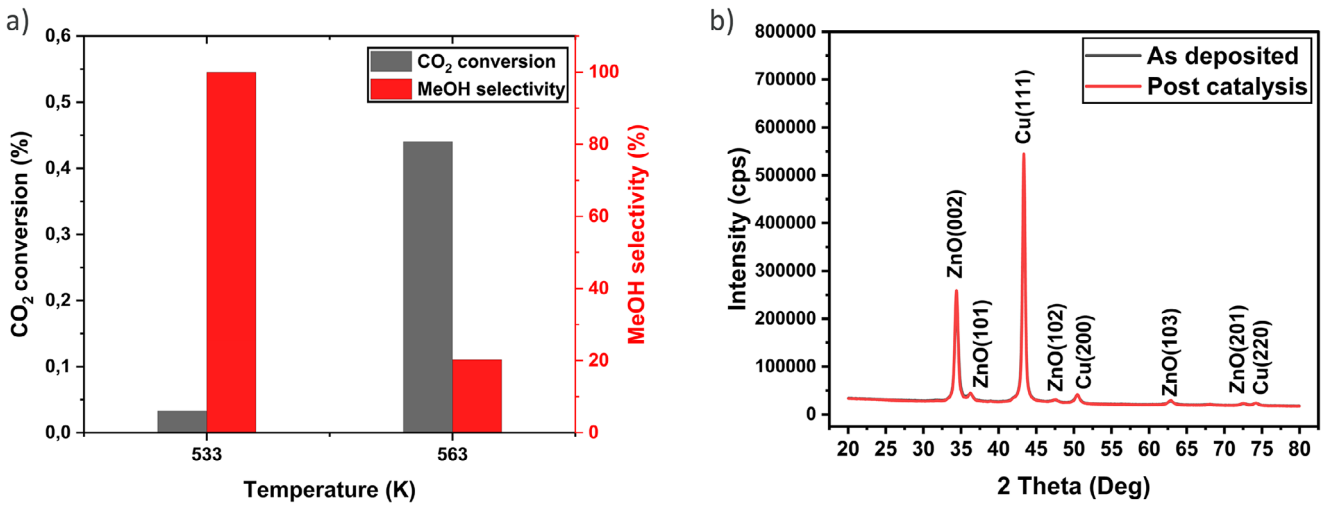


**Figure 4.** a) $CO_2$ conversion and MeOH selectivity as a function of temperature at P = 30 bar, flow = 25 mL $min^{-1}$, $CO_2$:$H_2$:$N_2$ = 1:3:1, b) XRD diffractogram of the Cu/ZnO multilayer catalyst before and after $CO_2$ hydrogenation.

potential mass transfer limitations associated with the microstructured geometry. Nonetheless, the ability to systematically engineer and expose buried metal–metal oxide interfaces provides a valuable platform for mechanistic studies and rational catalyst design. Future work will focus on optimizing the interfacial density, introducing secondary oxide modifiers, and enhancing gas–solid contact to improve catalytic productivity. However, methanol selectivity decreased sharply with rising temperature, dropping from nearly 100% at 533 K to ≈ 20% at 563 K. This trend is explained by the thermodynamics of methanol synthesis, where higher temperatures favour side reactions, such as the reverse water-gas shift reaction, leading to CO formation instead of methanol.[42,44] These findings align with theoretical studies highlighting temperature-sensitive regulation of active sites and the competition between methanol synthesis and Reverse Water Gas Shift pathways.[9] Moreover, catalyst support and structure, such as the interaction of silica or ZnO with Cu, have also been shown to influence methanol selectivity under varying reaction temperatures.[45] These results highlight the inherent challenge of balancing conversion and selectivity, emphasizing the need for optimizing reaction conditions, such as intermediate temperatures and pressures, to achieve better performance.[43]

To assess the structural evolution of the Cu/ZnO multilayer catalyst under reaction conditions, we performed post-catalysis XRD analysis and compared the results to the as-deposited state (Figure 4b). Crystallite sizes were estimated using the Scherrer equation based on the (002) reflection of ZnO and the (111) reflection of Cu. Following catalysis, the ZnO crystallite size increased from 12.16 nm to 13.63 nm, and the Cu crystallite size increased from 15.17 to 16.58 nm, corresponding to moderate growth of ≈12% and 9%, respectively. This trend is consistent with thermally induced recrystallization of ZnO and the onset of Cu grain coalescence under high-pressure, high-temperature hydrogenation conditions, as also reported for ZnO-based and Cu–ZnO systems under thermal treatments.[20,33] In addition to crystallite growth, the post-catalysis XRD pattern exhibited a slight increase in the intensity of both ZnO (002) and Cu (111) peaks, accompanied by narrowing of the full width at half maximum (FWHM). This peak sharpening suggests improved crystallinity and reduced microstructural disorder, rather than amorphization, defect formation, or surface reconstruction. Furthermore, two additional reflections at 72.53° and 74.29° were observed in the samples tested for catalysis, corresponding to the ZnO (201) and Cu (220) planes, respectively. These peaks were not present in the XRD data from samples used to study laser ablation effects, which contained only 20 layers, indicating that the emergence of these higher-order reflections is enabled by the increased layer count and improved long-range order in the 250-layer architecture. The absence of new phases and the consistent peak positions further support that no phase transformation occurred during the reaction. These findings confirm that the multilayer architecture retains its crystallographic integrity and resists structural degradation under catalytic conditions, which is particularly important for maintaining performance in slow interfacial reactions such as $CO_2$ hydrogenation to methanol.[9,15,19]

The methodology presented here, while demonstrated for $CO_2$ hydrogenation, offers a versatile platform that can be extended to a wide range of chemical reactions occurring at metal/metal-oxide interfaces. Unlike previous approaches such as the one by Frei et al.,[15] which were limited to static single-interface geometries, our multilayer architecture enables unprecedented flexibility in tailoring the interface properties. For example, by incorporating intermediate layers such as $Al_2O_3$ or $ZrO_2$ between Cu and ZnO films, one can modulate interfacial chemistry, electronic interactions, and defect structures in a controlled and systematic manner. In fact, defect-engineered oxide systems such as Fe-doped $CeO_2$ have recently demonstrated promising activity in tandem $CO_2$ hydrogenation reactions, attributed to controlled oxygen vacancy formation.[46] This opens new opportunities not only for optimizing catalytic performance but also for probing fundamental mechanistic questions such as validating or refuting hydrogen spillover hypotheses by strategically introducing insulating spacers that disrupt direct metal-metal oxide contact. Moreover, the individual thin-film parameters such as thickness, crystallinity, dopant concentration, and layer sequence can be precisely controlled using established protocols from PV and

microelectronics thin-film technologies. The scalability of this approach is also promising: RF magnetron sputtering is already widely used in industry, and its adaptation to roll-to-roll platforms would allow cost-effective deposition of multilayer films over large areas with high reproducibility.[47] Complementarily, automated laser scribing systems, with processing speeds reaching up to 1000 mm $s^{-1}$, enable rapid and localized interface exposure, aligning with industrial-scale throughput requirements. Thus, this multilayer strategy serves not only as a powerful research tool for fundamental catalysis studies but also as a scalable and tunable approach for designing next-generation catalytic systems for energy conversion, sustainable chemical production, and environmental applications.

## 3. Conclusion

In this study, we aimed to develop a high interfacial density Cu–ZnO multilayer catalyst for $CO_2$ hydrogenation to methanol by integrating thin-film deposition with laser-based microstructuring. To the best of our knowledge, this represents the first demonstration of a multilayer catalyst system fabricated using scalable RF magnetron sputtering and picosecond laser scribing to create accessible Cu–ZnO interfaces for gas-phase catalysis. Using a custom-designed split target, alternating nanometer-thick layers of Cu and ZnO were deposited by RF sputtering, followed by laser scribing under optimized power and velocity conditions to generate well-defined microstructures that expose buried interfaces. Comprehensive characterization by AFM, XRF, XRD, XPS, and SEM confirmed excellent layer definition, minimal interdiffusion, and both thermal and chemical stability. Through controlled roughness management and stacking strategies, we realized a multilayer architecture with substantially enhanced interfacial density. When tested in a Berty reactor, the catalyst achieved a $CO_2$ conversion of 0.45% at 563 K and nearly 100% methanol selectivity at 533 K. While demonstrated here for methanol synthesis, this methodology can be readily extended to other interface-driven catalytic reactions. The use of industry relevant, scalable techniques underscores the practical potential of this approach as a model platform for studying interface driven reactions, and potentially integrating with larger scale catalyst architectures in future designs. Future studies will focus on benchmarking against powder-based systems, long-duration testing, and operando studies to validate the durability and mechanistic uniqueness of the structured multilayer catalyst platform.

## 4. Experimental Section

*Catalyst Preparation*: Catalysts were prepared on Corning Eagle XG (boro-aluminosilicate) glass substrates of 0.7 mm thickness from Siegert wafer GmbH (Germany). First, the factory cleaned glasses were manually scribed to the required dimensions *i.e* 15 mm × 10 mm and then cut to the desired pieces. A Nitrogen blow was used to remove the dust and small glass pieces on the surface. The deposition of the catalytic layers was performed using a combined Physical Vapour Deposition (PVD)/ Chemical Vapour Deposition (CVD) cluster tool CS400PS from Von-Ardenne GmbH (Germany). Radio Frequency magnetron sputtering was utilized from a 10-inch magnetron source, which was equipped with a split target consisting of semicircular Cu and ZnO plates on a single copper backplate with a diameter of 24 cm. This approach significantly reduced fabrication time from days to just a few hours, an improvement over conventional methods using separate targets, which are more complex and time-consuming. The samples were deposited at room temperature utilizing an RF power of 400 W or power density of 1.76 W.$cm^{-2}$. The argon flow rate was maintained at 50 sccm, with a working pressure of 2 Pa, and the substrate-to-target distance was set at a minimum distance of 5 cm to reduce the cross talk between the materials. After multilayer deposition a $SiO_2$ layer was deposited by Plasma Enhanced Chemical Vapour Deposition (PECVD) at 300 °C using $SiH_4$ and $N_2O$ as precursors, this was done to eliminate any potential catalytic activity from the top surface. In order to expose the interfacial regions essential for catalytic activity, laser ablation process based on a diode-pumped solid-state (DPSS) Nd:$YVO_4$ picosecond laser with a wavelength of 1064 nm was employed. The laser scribing process was conducted under two distinct parameter regimes to achieve different structural morphologies. For the creation of cuboidal pillar-like structures, the laser was operated at 10% of its maximum power with energy of 15.9 µJ (Table S2, Supporting Information), with a pulse repetition rate of 25 kHz. The scribing velocity was maintained at 50 $mms^{-1}$. The formation of inverse structures (circular holes) was achieved by increasing the laser power to 100% of its maximum value with energy of 146.3 µJ (Table S2, Supporting Information), and lowering the repetition rate to 2 kHz, while increasing the scribing velocity to 500 $mms^{-1}$ to get single, spatially separated shots of laser.

*Characterizations*: The thickness of the deposited films was determined with Contact Profilometry using a DektakXT Profilometer from Bruker. A stylus force of 3 mg was applied, and a scan length of 2000 µm was used, covering both the film and the substrate to accurately measure the step height. Surface roughness and 3D topographic profiles were obtained via Atomic Force Microscopy (AFM) on a Park XE-70 system in non-contact mode, with a scan size of 10 µm × 10 µm and a scan rate of 0.2 Hz. The acquired data were processed using Gwyddion software[48] which was also used to find the Root mean square (RMS) roughness (Rq) and peak to valley height (Sz). The elemental composition of the films was analyzed using X-ray Fluorescence (XRF) on a Rigaku ZSX Primus II system, employing the quantitative analysis method. The measurements were performed using a sample holder with a diameter of 10 mm, ensuring precise alignment and accurate determination of the elemental composition. The surface composition and element oxidation states were examined using X-ray Photoelectron Spectroscopy (XPS) with a CLAM 4 spectrometer, employing Mg K$\alpha$ radiation (1253.6 eV) generated by a Specs XR50 X-ray gun and calibrated with Au 4f. The peaks were calibrated using the C 1s peak at 284.8 eV as a reference. The peaks were deconvoluted using Fityk software[49] with a Voigt function, which incorporates both Gaussian and Lorentzian components, and later was further processed and plotted using Origin Pro software.[50] The surface morphology and cross-sectional interface were studied using a Keyence VK-X250 Confocal Laser Microscope and a Zeiss Merlin Gemini 2 Scanning Electron Microscope (SEM). The crystal structure was assessed using X-ray Diffraction (XRD) in Bragg-Brentano geometry with a $2\theta$ range of 20°–80° and step size of 0.07 on a PANalytical system equipped with a Cu K$\alpha$ radiation source ($\lambda = 1.5406$ Å). Crystallite sizes of Cu and ZnO were estimated using the Scherrer Equation (1):

$$D = \frac{K\lambda}{\beta cos\theta} \quad (1)$$

where $D$ is the average crystallite size, $K$ is the shape factor (0.9), $\lambda$ is the X-ray wavelength (0.15406 nm for Cu K$\alpha$ radiation), $\beta$ is the Full Width at Half Maximum (FWHM) in radians, and $\theta$ is the Bragg angle. FWHM values were extracted by Gaussian fitting of the ZnO (002) and Cu (111) peaks. Instrumental broadening was assumed negligible.

Microstrain ($\epsilon$) was calculated using the relation:

$$\varepsilon = \frac{\beta}{4tan\theta} \quad (2)$$

This relation accounts for lattice distortions contributing to peak broadening. Background-subtracted FWHM values were used to evaluate the influence of laser scribing. A Williamson–Hall plot is also included in the Supplementary Information (Figure S2, Supporting Information) to

support the size–strain analysis. The diffraction peaks were identified using Match! software[51] by comparing the experimental data with reference patterns from the International Centre for Diffraction Data (ICDD) database.

*Catalytic Measurements*: The catalytic performance of the multilayer Cu-ZnO system for $CO_2$ hydrogenation to methanol reaction was evaluated using a lab-scale, gradient-free Berty reactor[52] (1-inch I.D. Micro Catalytic Fixed-basket Reactor, Autoclave Engineers, USA) with a total reactor volume of 50 mL. The reactor was equipped with a fixed sample basket and an internal stirrer rotating at 2500 RPM. Eight samples, each measuring 15 × 10 mm and consisting of 250 layers, were mounted in a specially designed sample holder (inner diameter: 15.85 mm, see Figure S5, Supporting Information) made of AISI 316Ti stainless steel. The experiments were conducted at a total pressure of 30 bar, with a continuous gas flow rate of 25 mL.min$^{-1}$ (Figure S6, Supporting Information). The total measured weight of the material deposited on glass was ≈39 mg (Table S3, Supporting Information), corresponding to a Weight Hourly Space Velocity (WHSV) of 38.5 h$^{-1}$. The catalyst mass was determined by weighing the glass substrates before and after film deposition using a Sartorius CPA224S microbalance with a resolution of 0.01 mg. The reactants mixture of $CO_2$:$H_2$:$N_2$ = 1:3:1 (Linde GmbH, Germany) is supplied with the flow rates precisely regulated using mass flow controller (MFC) EL-FLOW Prestige (Bronkhorst Deutschland Nord GmbH). The product stream was analyzed using an online Micro Gas chromatograph (μGC 490, Agilent, US), equipped with CP-Molsieve 5Å and PoraPLOT Q columns, along with heated sample lines and injectors to ensure accurate analysis.[53] The gas composition at the reactor inlet and outlet was analyzed to determine the mole fractions of $CO_2$ and reaction products (e.g., MeOH, CO, $H_2O$). $CO_2$ conversion was calculated based on the inlet and outlet molar flow rates using Equation (3):

$$CO_2\ conv.\ (\%) = \frac{F_{CO2,in} - F_{CO2,out}}{F_{CO2,in}} \times 100 \quad (3)$$

where $F_{CO2,in}$ and $F_{CO2,out}$ are the molar flow rates of $CO_2$ at the inlet and outlet, respectively. These were obtained by multiplying the total flow rate by the respective mole fractions of $CO_2$. Methanol and CO selectivity were calculated as the fraction of converted $CO_2$ that was transformed into methanol or CO, respectively, using:

$$Selectivity\ (\%) = \frac{Moles\ of\ desired\ product}{Moles\ of\ CO_2\ converted} \times 100 \quad (4)$$

*Data Reconciliation*: In the $CO_2$ hydrogenation to methanol experiments, the raw concentration data obtained from the micro gas chromatograph (μGC) is subject to measurement errors. These errors often lead to inconsistencies such as mole or mass fractions not summing to one, which violates fundamental physical constraints. To address this, a data reconciliation approach is used, leveraging the fact that the system is governed by a single. The reconciliation process ensures that the final dataset adheres to elemental balances for carbon (C), hydrogen (H), oxygen (O), and nitrogen (N), as well as summation constraints that require the total mole or mass fractions at both the reactor inlet and outlet to be equal to one. This optimization is performed using the *fmincon* solver in Matlab, which minimizes the deviation between the measured and reconciled values while satisfying the constraints.

The objective function is defined as:

$$\min f(x) = \sum (x_{meas} - x_{calc})^2 \quad (5)$$

where $x_{meas}$ are the raw measurements and $x_{calc}$ are the adjusted (reconciled) values.

The solution is subject to a set of nonlinear equality constraints $g$:

$$g(x) = 0 \quad (6)$$

## Supporting Information

Supporting Information is available from the Wiley Online Library or from the author.

## Acknowledgements

The authors would like to thank Martin Muske, Tobias Kohler, Meysam Khodabakshi, Nicolas Jannik Otto, Florian Ruske, and Rene Schwidessen for their help and support during measurements. The authors acknowledge the support from the German Federal Ministry of Research, Technology and Space in the Framework of the Project Catlab (03EW0015A). This work was also partially funded by the Deutsche Forschungsgemeinschaft (DFG, German Research Foundation) under Germany's Excellence Strategy (EXC 2008—390540038) UniSysCat and Einstein Foundation Berlin.

## Conflict of Interest

The authors declare no conflict of interest.

## Data Availability Statement

The data that support the findings of this study are available from the corresponding author upon reasonable request.

## Keywords

$CO_2$ hydrogenation, Cu-ZnO, heterogeneous catalysis, interface, laser scribing

Received: June 3, 2025
Revised: June 27, 2025
Published online: July 14, 2025

[1] G. Ertl, *Angew. Chem. Int. Ed.* **2008**, *47*, 3524.
[2] G. A. Olah, *Angew. Chem. – Int. Ed.* **2005**, *44*, 2636.
[3] M. Bukhtiyarova, T. Lunkenbein, K. Kähler, R. Schlögl, *Catal. Lett.* **2017**, *147*, 416.
[4] R. S. Swathi, K. L. Sebastian, *Reson.* **2008**, *13*, 548.
[5] N. M. Deraz, *Ind. Environ. Chem.* **2018**, *2*, 19.
[6] L. Cao, J. Lu, *Catal. Sci. Technol.* **2020**, *10*, 2695.
[7] R. Paudel, A. R. Burton, M. A. Kuroda, B. H. Farnum, R. B. Comes, *J. Vac. Sci. Technol. A* **2023**, *41*, 063207.
[8] Z. Li, E. Öztuna, K. Skorupska, O. V. Vinogradova, A. Jamshaid, A. Steigert, C. Rohner, M. Dimitrakopoulou, M. J. Prieto, C. Kunkel, M. Stredansky, P. Kube, M. Götte, A. M. Dudzinski, F. Girgsdies, S. Wrabetz, W. Frandsen, R. Blume, P. Zeller, M. Muske, D. Delgado, S. Jiang, F.-P. Schmidt, T. Köhler, M. Arztmann, A. Efimenko, J. Frisch, T. M. Kokumai, R. Garcia-Diez, M. Bär, et al., *Nat. Commun.* **2024**, *15*.
[9] L. Zhang, C. Li, Y. Liu, C. Xu, Y. Zhang, *npj Comput. Mater.* **2024**, *10*, 10660.
[10] W. Liao, C. Tang, H. Zheng, J. Ding, K. Zhang, H. Wang, J. Lu, W. Huang, Z. Zhang, *J. Catal.* **2022**, *407*, 126.
[11] I. Ro, J. Qi, S. Lee, M. Xu, X. Yan, Z. Xie, G. Zakem, A. Morales, J. G. Chen, X. Pan, D. G. Vlachos, S. Caratzoulas, P. Christopher, *Nature* **2022**, *609*, 287.
[12] S. M. Kim, H. Lee, J. Y. Park, *Catal. Lett.* **2015**, *145*, 299.
[13] P. C. Stair, *Nat. Chem.* **2011**, *3*, 345.
[14] L. Zou, J. Li, D. Zakharov, E. A. Stach, G. Zhou, *Nat. Commun.* **2017**, *8*, 307.

[15] M. S. Frei, F. L. P. Veenstra, D. Capeder, J. A. Stewart, D. Curulla-Ferré, A. J. Martín, C. Mondelli, J. Pérez-Ramírez, *Small Methods* **2021**, *5*, 2001231.
[16] J. R. Rostrup-Nielsen, In *Progress in Catalyst Deactivation* (Ed: J. L. Figueiredo), NATO Advanced Study Institutes Series, Vol. *54*, Springer, Dordrecht **1982**, pp. 209–227, https://doi.org/10.1007/978-94-009-7597-2_11.
[17] W. Arabczyk, R. Pelka, I. Jasińska, Z. Lendzion-Bieluń, *Crystals (Basel)* **2024**, *14*, 188.
[18] A. Gili, L. Schlicker, M. F. Bekheet, O. Görke, S. Penner, M. Grünbacher, T. Götsch, P. Littlewood, T. J. Marks, P. C. Stair, R. Schomäcker, A. Doran, S. Selve, U. Simon, A. Gurlo, *ACS Catal.* **2018**, *8*, 8739.
[19] A. Gili, G. Brösigke, M. Javed, E. Dal Molin, P. Isbrücker, J.-U. Repke, F. Hess, A. Gurlo, R. Schomäcker, M. F. Bekheet, *Angew. Chem. – Int. Ed.* **2025**, *64*, 202416990.
[20] M. Saito, K. Murata, *Catal. Sur. Asia* **2004**, *8*, 285.
[21] K. Xiao, Q. Wang, X. Qi, L. Zhong, *Catal. Lett.* **2017**, *147*, 1581.
[22] A. Wucher, W. Reuter, *J. Vac. Sci. Technol. A* **1988**, *6*, 2316.
[23] M. K. Gora, A. Kumar, S. Kumar, P. K. Maheshwari, D. patidar, S. N. Dolia, R. K. Singhal, *Environ. Sci. Pollut. Res.* **2023**, *30*, 98632.
[24] Z. Jehl, M. Bouttemy, D. Lincot, J. F. Guillemoles, I. Gerard, A. Etcheberry, G. Voorwinden, M. Powalla, N. Naghavi, *J. Appl. Phys.* **2012**, *111*, 114509.
[25] M. Trost, S. Schröder, C. C. Lin, A. Duparré, A. Tünnermann, *Proc. SPIE* **2012**, *8501*, 85010F.
[26] A. Arman, Ş. Ţălu, C. Luna, A. Ahmadpourian, M. Naseri, M. Molamohammadi, *J. Mater. Sci.: Mater. Electron.* **2015**, *26*, 9630.
[27] K. Kandpal, J. Singh, N. Gupta, C. Shekhar, *J. Mater. Sci.: Mater. Electron.* **2018**, *29*, 14501.
[28] V. Kumar, S. K. Singh, H. Sharma, S. Kumar, M. K. Banerjee, A. Vij, *Phys. B Condens. Matter* **2019**, *552*, 221.
[29] A. I. Istrate, I. Mihalache, C. Romanitan, O. Tutunaru, R. Gavrila, V. Dediu, *J. Mater. Sci.: Mater. Electron.* **2021**, *32*, 4021.
[30] B. Stegemann, C. Schultz, *Digital Encyclopedia of Applied Physics* **2019**.
[31] A. D. Compaan, I. Matulionis, M. J. Miller, U. N. Jayamaha, Conference Record of the Twenty Fifth IEEE Photovoltaic Specialists Conference, Washington, DC, USA **1996**, pp. 769–772, https://doi.org/10.1109/PVSC.1996.564241.
[32] P. Zhou, H. Liu, L. Zhang, X. Suo, Z. Liang, Y. Liu, Y. Li, Z. Jiang, Z. Wang, *J. Mater. Sci.: Mater. Electron.* **2016**, *27*, 7822.
[33] S. S. Fouad, L. I. Soliman, E. Baradács, M. E. Sayed, B. Parditka, N. F. Osman, M. Nabil, Z. Erdélyi, *J. Mater. Sci.* **2023**, *58*, 6632.
[34] S. S. Fouad, B. Parditka, M. Nabil, E. Baradács, S. Negm, Z. Erdélyi, *J. Mater. Sci.: Mater. Electron.* **2022**, *33*, 20594.
[35] B. Giroire, B. Giroire, M. Ali Ahmad, G. Aubert, L. Teule-Gay, D. Michau, J. J. Watkins, C. Aymonier, A. Poulon-Quintin, *Thin Solid Films* **2017**, *643*, 53.
[36] S. Lee, J. Y. Kim, T.-W. Lee, W.-K. Kim, B.-S. Kim, J. H. Park, J.-S. Bae, Y. C. Cho, J. Kim, M.-W. Oh, C. S. Hwang, S.-Y. Jeong, *Sci. Rep.* **2014**, *4*, 6230.
[37] J. A. Kim, J. H. Park, S. G. Park, C. S. Son, Y. G. Son, D. H. Hwang, *Crystals (Basel)* **2023**, *13*, 643.
[38] M. Sreedhar, I. N. Reddy, P. Bera, D. Ramachandran, K. Gobi Saravanan, A. M. Rabel, C. Anandan, P. Kuppusami, J. Brijitta, *Appl. Phys. A Mater. Sci. Process* **2015**, *120*, 765.
[39] J. Choi, R. Jung, *J. Korean Phys. Soc.* **2018**, *73*, 1546.
[40] A. Jilani, J. Iqbal, M. S. Abdel-wahab, Y. Jamil, A. A. Al-Ghamdi, *J. Optoelectron. Biomed. Mater.* **2016**, *8*, 27.
[41] S. Muthusamy, S. Bharatan, S. Sivaprakasam, R. Mohanam, *Materials* **2024**, *17*, 5153.
[42] U. J. Etim, Y. Song, Z. Zhong, *Front. Energy Res.* **2020**, *8*, 545431.
[43] R.-P. Ye, J. Ding, W. Gong, M. D. Argyle, Q. Zhong, Y. Wang, C. K. Russell, Z. Xu, A. G. Russell, Q. Li, M. Fan, Y.-G. Yao, *Nat. Res.* **2019**, *10*, 5698.
[44] A. Ramirez, X. Gong, M. Caglayan, S.-A. F. Nastase, E. Abou-Hamad, L. Gevers, L. Cavallo, A. Dutta Chowdhury, J. Gascon, *Nat. Commun.* **2021**, *12*, 5914.
[45] L. Wang, E. Guan, Y. Wang, L. Wang, Z. Gong, Y. Cui, X. Meng, B. C. Gates, F.-S. Xiao, *Nat. Commun.* **2020**, *11*, 1033.
[46] A. Gili, M. F. Bekheet, F. Thimm, B. Bischoff, M. Geske, M. Konrad, S. Praetz, C. Schlesiger, S. Selve, A. Gurlo, F. Rosowski, R. Schomäcker, *Catal. Sci. Technol.* **2024**, *14*, 4174.
[47] T. Segawa, Y. Ikari, N. Ooba, N. Kawakami, N. Jiko, H. Tao, *Kobelco Technol. Rev.* **2016**, *34*, 44.
[48] D. Nečas, P. Klapetek, *Open Phys.* **2012**, *10*, 181.
[49] M. Wojdyr, *J. Appl. Crystallogr.* **2010**, *43*, 1126.
[50] OriginLab Corporation, OriginPro, Version 2022b, Northampton, MA, USA, **2022**.
[51] H. Putz, *Match!—Phase Identification from Powder Diffraction*, Crystal Impact, Bonn, Germany **2025**.
[52] L. Thum, C. Marshall, G. von der Waydbrink, E. Stotz, K. Skorupska, R. Schlögl, *Chem. Ing. Tech.* **2025**, https://doi.org/10.1002/cite.70001.
[53] M. Javed, G. Brösigke, R. Schomäcker, J. U. Repke, *Chem. Eng. Technol.* **2023**, *46*, 1163.